Mirror Array Aided Indoor SSK Visible Light Downlink

Meng Lu, Fasong Wang, Rui Li, Ting Zuo, and Jiankang Zhang *Senior Member, IEEE*

Abstract

In indoor visible light communications (VLC) systems, line of sight (LoS) blockage severely impairs the received power of users. To address this issue, in this paper, a paradigm of indoor space shift keying (SSK) VLC system aided by mirror array is investigated. Firstly, the mirror array reflects the light signal received from LEDs to the user's photo-detector (PD) by the virtue of mirror reflection characteristics. And then, a method of power focusing is presented by adjusting the angle of the mirror according to the locations of LEDs and PDs. Additionally, the synchronous issue is analyzed theoretically to address the multipath effects. Furthermore, an orthogonal matching pursuit (OMP) detection algorithm aided by singular value decomposition (SVD) is proposed for the considered system. Finally, simulations are presented to verify the effectiveness of the proposed mirror array aided indoor SSK-VLC system.

Index Terms

Visible light communication (VLC), space shift keying (SSK), mirror array, orthogonal matching pursuit (OMP), maximum likelihood (ML)

I. Introduction

With the popularity of powerful and continuously connected mobile devices, a large number of devices need to process and connect the information in the Internet of Things (IoT)

M. Lu, F. Wang and T. Zuo are with the School of Information Engineering, Zhengzhou University, Zhengzhou, 450001, Henan, China. (e-mails: zhengdalumeng@126.com; iefswang@zzu.edu.cn; 15978370982@163.com)

R. Li is with the School of Sciences, Henan University of Technology, Zhengzhou, 450001, Henan, China. (e-mail: slxlr@haut.edu.cn)

J. Zhang is with the Department of Computing and Informatics, Bournemouth University, Bournemouth BH12 5BB, U.K. (e-mail: jzhang3@bournemouth.ac.uk)

This research was supported in part by the National Natural Science Foundation of Henan Province under Grant 222102210003, in part by the National Natural Science Foundation of China under Grant 61401401 and 61901366, and in part by the National Key Research and Development Program under Grant 2019QY0302. Corresponding authors: Fasong Wang(e-mail: iefswang@zzu.edu.cn)

era. Therefore, the ensuing problem is that the spectrum resources of traditional wireless communication are increasingly congested, leading to the existing spectrum resources in the environment with abundant demands has been gradually failed to meet the needs of people. In order to fundamentally solve the contradiction between super-large capacity demand and spectrum crisis, indoor VLC, as a promising wireless transmission technology, has attracted wide attention. By using visible spectrum without authorization, VLC can alleviate spectrum congestion in the radio frequency bands [1]–[3].

In indoor scenarios, since light cannot penetrate walls and other objects, the problems that often occur in indoor VLC systems are reflection and blocking of light propagation. Among them, diffuse reflection is more prominent because of the uncertain radiation mode of reflected light direction [4]. In previous VLC system studies, the communication network is more considered in line of sight (LoS) case, where the signals are sent directly from transmitter to receiver, which is usually used for point-to-point communication [5]. In order to alleviate this situation, non-LoS (NLoS) links are universally applied. However, in the diffuse reflection system of NLoS transmission, the optical path loss is more difficult to predict because it depends on multiple factors. Under normal circumstances, even the strongest NLoS component is still at least 7 dB lower than the LoS component after the light is diffusely reflected [6]. With the acceleration of transportation development, the subway, high-speed railway, and airplanes have become increasingly common modes of transport. In these three scenarios, there are usually equipped with many LEDs lighting devices, therefore, VLC can be easily adopted for convenience and security. However, due to the complexity of the usage environment, LoS blockage usually occurs. In addition, for unmanned equipment communicated by VLC, LoS link blocking is also common when they work in underground mines scenarios.

As energy and cost-efficient emerging technology, reconfigurable intelligent surfaces (RISs) [7] can be deployed on existing indoor infrastructure building walls to improve communication quality by configuring its elements to reflect any incident light from the LEDs to the receiver's PDs. At the same time, by taking advantage of the characteristics of RIS, the LoS communication requirements of indoor VLC systems can be relaxed. Then, various topics have been investigated to explore the performance of RISs aided optical communications. In a little more detail, based on an iterative time-efficient model, the performance of NLoS channel assisted by the first-order reflection of a fixed mirror was proposed in [8]. By utilizing RISs, a controllable multi-branch wireless communication based on optical RISs is proposed

for free-space optical communication [9]. By introducing a discrete matrix, the allocation of RISs is simplified into a binary programming problem, and a low-complexity algorithm that maximizes the sum rate in the case of multiple users is proposed [10]. Then, for RISs aided VLC system, [11] proposed a non-convex optimization problem for optimizing the configuration of RIS elements. Furthermore, aided by RISs, the security of VLC and VLC-RF systems are investigated in [12], [13].

Practically, due to the limited luminous flux of individual LEDs, multiple LEDs are usually deployed to obtain adequate illumination in a typical application space. The space shift keying (SSK) modulation technique is naturally befitted in indoor VLC systems by utilizing multiple LEDs. Thus SSK aided VLC systems have been extensively studied [14], [15]. In SSK-VLC systems, according to the input information bits, during one specific symbol duration, one LED is activated to transmit a specific information symbol, while the rest LEDs are only used for illumination. Naturally, these spatially distributed LEDs can be viewed as spatial constellation points, which can be utilized for conveying information. Therefore, the SSK modulation is absolutely suitable for VLC systems, and in this circumstance, the LEDs are used not only for data transmission but also for basic adequate lighting. However, to the best of our knowledge, there are no results in the literature for RIS aided SSK-VLC systems.

At the time of writing, the detection algorithms in the aforementioned indoor SSK-VLC system are mainly based on the ML method [16]. Although it is optimal in a sense, with the number of LEDs increasing at the transmitter, the computational complexity brought by ergodic searching will increase dramatically. Therefore, it is plausible to find an efficient detector with low computational complexity and ideal performance at the receiver. Inspired by the idea in [17], in this paper, an OMP detection algorithm based on compressive sensing (CS) and singular value decomposition (SVD) is utilized to realize the signal detection more efficiently.

Hence, a mirror array assisted indoor SSK-VLC downlink model is proposed in this paper. The proposed scheme is inspired by the fact that a mirror array with smooth surfaces can reflect light almost without loss. Furthermore, motivated by the sparsity nature of SSK signals, a corresponding low complexity detector is also presented. The proposed approach can overcome the problems of blocked light in the LoS link and the low-power characteristics of PDs in the NLoS link. The contributions of this paper can be summarized as follows:

- For the first time, the mirror array aided indoor SSK-VLC downlink model is proposed, which is realized by reflecting the light signal received from LEDs to the user's PDs by

the virtue of mirror reflection characteristic.

- A power focusing method is investigated by adjusting the angle of the mirror individually according to the locations of LEDs and PDs. It can be achieved by a central mechanical controller of the mirror reflector.
- The multipath fading and inter-symbol interference (ISI) issues are analyzed theoretically to address the multipath effects caused by different mirrors.
- Enabled by SVD, an OMP detection algorithm is proposed for the considered system, which has much lower computational complexity than ML.

The remainder of this paper is organized as follows: the system model is described in Section II. The multipath fading and ISI are discussed in detail in Section III. Section IV presents the OMP detector based on channel matrix preprocessing. Specific simulation results are given in section V. Finally, the conclusion is summarized in section VI.

II. The system model

A. Indoor VLC channel model assisted by mirror array

Due to the fact that the reflection on the surface of an object is determined by the composition of material and geometry, a smooth surface can act as a mirror. According to Snell theorem [18], when the smooth mirror reflects light, it follows that the angle of incidence is equal to the angle of reflection.

Assuming that LEDs are placed on the top of the service area, and the reflection of light by the mirror array fixed on the wall is specular reflection. The mirror array contains $M \times N$ mirrors with the same size, every size of the mirror is $w \times h$ cm^2. For the considered mirror array, a three-dimensional (3D) Cartesian coordinate system is built with the origin $O_{p,q}$ as the center of the p-th row and q-th column mirror of the array. It is assumed that the orientation of each mirror can be adjusted by independent rotation of two degrees of freedom. In order to avoid the light occlusion phenomenon occurring in mirror rotation, it is assumed that there is a certain transverse spacing Δw cm and longitudinal spacing Δh cm among adjacent mirrors. In addition, to realize the power focusing in the considered system with mirror array, it is also assumed that the final mirror direction can be realized by rotating the specific mirror clockwise twice [19].

The coordinate system considered in this paper is depicted in Fig. 1, assuming that the original coordinate system is $O_X - O_Y - O_Z$, by rotating around the axis Z with angle $\alpha_{p,q}$, the coordinate system $O_{X'} - O_{Y'} - O_{Z'}$ is attained and then the second rotation is

based on the coordinate system $O_{X'} - O_{Y'} - O_{Z'}$ by rotating $\beta_{p,q}$ around the axis X' to obtain $O_{X''} - O_{Y''} - O_{Z''}$. It is further assuming that the initial state of each mirror is set to $\alpha_{p,q} = 0$, $\beta_{p,q} = 0$, $\forall p, q$, and the rotational degree of the reflection mirror $\alpha_{p,q}$ and $\beta_{p,q}$ lie in $[-\pi/2, \pi/2]$. In our considered system, we assume that only one reflection by the mirror array is required to achieve our objectives. Under this circumstance, the mirror direction after each rotation can be determined by finding the normal vector $\mathbf{n}_{p,q}$ perpendicular to the reflection mirror. Noted that the normal vector $\mathbf{n}_{\mathbf{p,q}}$ of the mirror coincides with the rotated coordinate axis Y''.

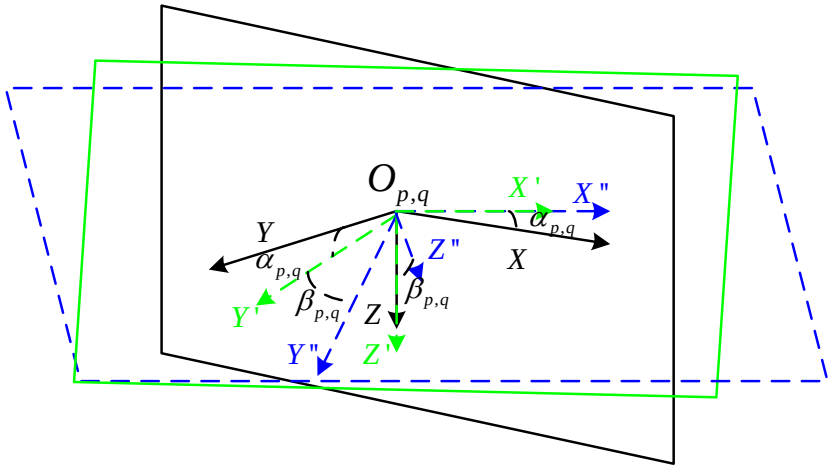

Fig. 1. The considered coordinate system of a mirror.

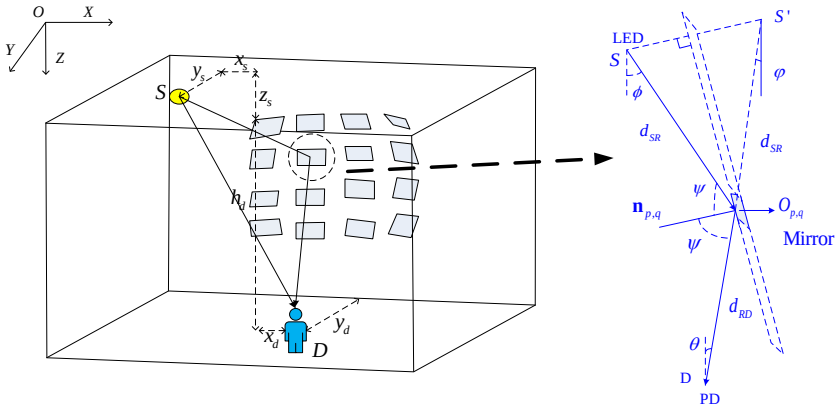

Fig. 2. Specular reflection mirror array model.

Firstly, the light reflected by the mirror located in the p-th row and the q-th column in the

mirror array is analyzed, as shown in Fig. 2, where S and D represent the LED and PD, respectively. A cartesian coordinate system is established with the center of the mirror as the origin, where Eq. (1) and Eq. (2) represent the positions of LED and PD, respectively.

$$\mathbf{s} = \begin{bmatrix} -\left(x_s + \frac{w}{2} + (q-1)\left(w+\Delta w\right)\right) \\ y_s \\ -\left(z_s + \frac{h}{2} + (p-1)\left(h+\Delta h\right)\right) \end{bmatrix}, \tag{1}$$

$$\mathbf{d} = \begin{bmatrix} x_d - (\frac{w}{2} + (q-1)(w+\Delta w)) \\ y_d \\ h_d - (\frac{h}{2} + (p-1)(h+\Delta h)) \end{bmatrix}, \tag{2}$$

where x_s, y_s, z_s are the coordinate distances between the mirror in the first row and the first column of the mirror array and the position of LED respectively; x_d, y_d, h_d are the coordinate distances between the mirror in the first row and column of the mirror array and the position of PD respectively. When the mirror realizes power focusing, the direction of normal vector $\mathbf{n}_{p,q}$ is given as follows [20]

$$\mathbf{n}_{p,q} = \frac{\mathbf{e}_{\overrightarrow{O_{p,q}S}} + \mathbf{e}_{\overrightarrow{O_{p,q}D}}}{\sqrt{2 + 2\mathbf{e}_{\overrightarrow{O_{p,q}S}}{}^{T}\mathbf{e}_{\overrightarrow{O_{p,q}D}}}}, \tag{3}$$

where $\overrightarrow{O_{p,q}S}$ represents the corresponding ray incident direction, $\mathbf{e}_{\overrightarrow{O_{p,q}S}}$ is the unit vector in the direction of vector $\overrightarrow{O_{p,q}S}$, and the unit vector $\mathbf{e}_{\overrightarrow{O_{p,q}D}}$ represents the direction of the ray's departure. Indeed, the normal vector $\mathbf{n_{p,q}}$ of the mirror in Fig. 2 coincides with the rotated coordinate axis Y'' in Fig. 1. Thus, rotating angles $\alpha_{p,q}$ and $\beta_{p,q}$ in Fig. 1 correspond to the rotation angles with respect to the mirror normal vector $\mathbf{n_{p,q}}$ concerning the coordinate system $O_X - O_Y - O_Z$ in Fig. 2. Then, the deflection angle with respect to the normal vector $\mathbf{n_{p,q}}$ of the mirror in Fig. 2 can be expressed as

$$\beta_{p,q} = \sin^{-1}(\mathbf{n}_{p,q}^{T}\mathbf{e_3}), \tag{4}$$

$$\alpha_{p,q} = \sin^{-1}\left(\frac{1}{\cos\beta_{p,q}}\mathbf{n}_{p,q}^{T}\mathbf{e_1}\right), \tag{5}$$

where $\mathbf{e_1}$ and $\mathbf{e_3}$ represent the unit vector of X axis and Z axis respectively.

Since the mirror array surface preserves an oriented and concentrated specular reflection property, the reflection points of the mirror do not conform to the lambert model. Hence, it is difficult to consider the multipath impulse response of mirror reflection using iterative calculation methods, however, we can model the specular reflection path as LoS blocked

by the ideal mirror [8]. Assume that S' is the mirror point of LED with respect to mirror symmetry, and the original reflection path is blocked by the mirror. At this point, the ray path can be regarded as LoS from mirror point S' to point D, as shown in Fig. 2.

To facilitate the calculation of LED image S', another cartesian coordinate system is defined, which still takes the center $O_{p,q}$ of the p-th row and the q-th column in the mirror array as the origin of coordinate. The new coordinate system is $O_{X''} - O_{Y''} - O_{Z''}$, which represents the rotated coordinate axes of the original $O_X - O_Y - O_Z$ as shown in Fig. 2. The transformation between the two cartesian coordinate systems is proposed as follows [21]

$$[A_{X''}, A_{Y''}, A_{Z''}]^T = \left(\mathbf{R}_{p,q}^{X'}\mathbf{R}_{p,q}^{Z}\right)^T [A_X, A_Y, A_Z]^T, \tag{6}$$

where $A_{X''}$, $A_{Y''}$ and $A_{Z''}$ are the coordinates of randomly selected point A relative to cartesian coordinate system $O_{X''} - O_{Y''} - O_{Z''}$, respectively, and their coordinates relative to cartesian coordinate system $O_X - O_Y - O_Z$ are A_X, A_Y and A_Z. $\mathbf{R}_{p,q}^{Z}$ represents the rotation matrix of $\alpha_{p,q}$ rotated clockwise around the axis Z, which can be expressed as

$$\mathbf{R}_{p,q}^{Z} = \begin{bmatrix} \cos(\alpha_{p,q}) & \sin(\alpha_{p,q}) & 0 \\ -\sin(\alpha_{p,q}) & \cos(\alpha_{p,q}) & 0 \\ 0 & 0 & 1 \end{bmatrix}. \tag{7}$$

Similarly, $\mathbf{R}_{p,q}^{X'}$ represents the rotation matrix of $\beta_{p,q}$ rotated clockwise around the axis of X', which can be expressed as $\mathbf{R}_{p,q}^{X'} = [\mathbf{r}_1, \mathbf{r}_2, \mathbf{r}_3]$, where

$$\mathbf{r}_1 = \begin{bmatrix} \cos^2(\alpha_{p,q})(1 - \cos(\beta_{p,q})) + \cos(\beta_{p,q}) \\ -\cos(\alpha_{p,q})\sin(\alpha_{p,q})(1 - \cos(\beta_{p,q})) \\ \sin(\alpha_{p,q})\sin(\beta_{p,q}) \end{bmatrix}, \tag{8}$$

$$\mathbf{r}_2 = \begin{bmatrix} -\cos(\alpha_{p,q})\sin(\alpha_{p,q})(1 - \cos(\beta_{p,q})) \\ \sin^2(\alpha_{p,q})(1 - \cos(\beta_{p,q})) + \cos(\beta_{p,q}) \\ -\cos(\alpha_{p,q})\sin(\beta_{p,q}) \end{bmatrix}, \tag{9}$$

$$\mathbf{r}_3 = \begin{bmatrix} \sin(\alpha_{p,q})\sin(\beta_{p,q}) \\ \cos(\alpha_{p,q})\sin(\beta_{p,q}) \\ \cos(\beta_{p,q}) \end{bmatrix}. \tag{10}$$

As aforementioned analysis, during the process of indoor mirror array aided SSK-VLC, the rotation of individual mirrors can be realized through electro-mechanical controller [19],

which controls the rotation angle provided by Eq. (6) and is installed on each mirror. For the nanoscale of visible light, it can provide high spatial resolution to accurately control the reflection direction. Additionally, we assume that the mirror array will not work when the LoS link is not blocked. Otherwise, when the LoS link is blocked, the controller controls the mirror array to enable communication.

B. Indoor SSK-VLC system model

The indoor VLC communication system considered in this paper adopts the typical MIMO-VLC system model. SSK, as a special MIMO technology without extra power consumption, only needs to activate one transmitting LED during each information transmission. When the number of transmitter LEDs is N_t, the SSK system can transmit high-speed data up to $\lfloor \log_2 N_t \rfloor$ bps/Hz, where $\lfloor \cdot \rfloor$ indicates the floor operation. Given that there are N_t LEDs at the top of the service area, assuming that the user is on a horizontal plane and has N_r PDs, the signals transmitted by the LEDs reach the PDs after power focusing through the mirror array, then the MIMO channel matrix is referred to as $\mathbf{H}$, and the entries of $\mathbf{H}$ is denoted as h_{ij}, which is the channel gain between the j-th LED transmitting signal and the i-th PD after the power focusing of the mirror array. Then the signal received by the receiving end is

$$\mathbf{y} = \mathbf{H}\mathbf{x} + \mathbf{n}, \tag{11}$$

where $\mathbf{x} = [x_1, x_2, ..., x_{N_t}]^T$ is the transmitted signal vector of dimension $N_t \times 1$, $\mathbf{n}$ is the Gaussian white noise vector with dimensional $N_r \times 1$.

III. The multipath fading and inter-symbol interference (ISI) issues

The communication links of individual mirrors in the mirror array are modeled as linear attenuation and delay based on the short-distance LoS and reflection characteristics of the mirrors [22], and then the optical links are considered as Dirac-like pulse. Consequently, for the considered indoor VLC downlink assisted by mirror array, the impulse response of the mirror reflection link at the p-th row and q-th column mirror and the total channel impulse response can respectively be expressed as

$$h_{p,q}^{(\mathrm{MI})}(t) = \frac{A(k+1)}{2\pi} \frac{\rho_{\mathrm{MI}}}{(d_{p,q})^2} \cos^k(\varphi) \cos(\theta) \,\mathrm{rect}\left(\frac{\theta}{\mathrm{FOV}}\right) \delta\left(t - \frac{d_{p,q}}{c}\right). \tag{12}$$

$$h^{(\mathrm{MI})}(t)=\sum_{p=1}^{M}\sum_{q=1}^{N}h_{p,q}(t), \tag{13}$$

where A is the effective area of PD that receives light source, k is the modulus of the radiation lobe, which is measured by $k=\frac{-\ln 2}{\ln(\cos\Phi_{1/2})}$ with half irradiance at semi-angle $\Phi_{1/2}$, $\mathrm{rect}(\cdot)$ function indicates that PD cannot receive optical signal when the incident angle of PD is greater than FOV, and then the channel gain $h_{p,q}^{(\mathrm{MI})}(t)$ between LED and PD is 0 in this case. ρ_{MI} is the specular reflection coefficient, and

$$d_{p,q}=d_{\mathrm{SO}_{p,q}}+d_{\mathrm{O}_{p,q}\mathrm{D}}, \tag{14}$$

where $d_{\mathrm{SO}_{p,q}}$ is the distance between the light source LED and the p-th row and q-th column reflecting mirror, $d_{\mathrm{O}_{p,q}\mathrm{D}}$ is the distance between receiving end PD and the p-th row and q-th column reflecting mirror. θ and φ are the receiving angle of receiver PD and the incidence angle of the imaginary lighting source S', respectively, and then we have

$$\cos(\theta)=\mathbf{e}_3^T\mathbf{e}_{\overrightarrow{\mathrm{O}_{p,q}\mathrm{D}}}, \tag{15}$$

$$\cos(\varphi)=\mathbf{e}_3^T\mathbf{e}_{\overrightarrow{\mathrm{S'}_{p,q}\mathrm{D}}}. \tag{16}$$

And finally, c is the speed of light.

Then, the channel gain of VLC system assisted by mirror array can be expressed as

$$H^{(\mathrm{MI})}(f)=\int_{-\infty}^{\infty}h^{(\mathrm{MI})}(t)\,dt=\sum_{p=1}^{M}\sum_{q=1}^{N}\eta_{\mathrm{MI}}e^{j2\pi f t_{p,q}}, \tag{17}$$

where

$$\eta_{\mathrm{MI}}=\frac{A(k+1)}{2\pi}\frac{\rho_{\mathrm{MI}}}{(d_{p,q})^2}\cos^k(\varphi)\cos(\theta)\,\mathrm{rect}\left(\frac{\theta}{\mathrm{FOV}}\right), \tag{18}$$

and $t_{p,q}=\frac{d_{p,q}}{c}$ denotes the transmission time taken by the signal from LED to the receiving end PD through the mirror in the p-th row and q-th column in the mirror array. In VLC, the carrier information signal has a frequency of about 10^{14} Hz, and the area of receiver PD is about millions of square wavelengths, therefore, the considered indoor VLC system is effectively not subject to multipath fading [23]. However, multipath propagation of emitted signals in the considered mirror array aided indoor VLC system may lead to inter-symbol interference (ISI), which will limit the transmission rate [24], [25]. Below, we will analyze this problem in depth and show that the possible ISI incurred by mirror array to the system can also be ignored.

The signal intensity received on the PD surface includes contributions from mirrors, as well as the NLoS components from reflections of walls or objects within the room when the LoS is blocked. It should be noted that the total received optical power of the LoS link at the receiver exceeds 95%, and even the strongest NLoS component is still at least 7 dB lower than that of the LoS component [23]. Consequently, we can neglect the NLoS components, but consider only the reflected components of the mirror array for carrying out tractable analysis.

Here, we first discuss the possible multipath effects incurred by the mirror array. When the positions of LEDs and PDs are fixed in the room, the optical signal is reflected in the receiving end PD by $M \times N$ mirrors, resulting in multiple optical paths. Then, the maximum delay spread Δt can be expressed as

$$\Delta t = \max\left\{t_{p,q}\right\} - \min\left\{t_{p,q}\right\}, \tag{19}$$

where $t_{p,q}$ denotes the signal transmission time from the activated LED to the receiver PD by the mirror reflection link at the p-th row and q-th column of the mirror array, and $p \in \{1, 2, \cdots, M\}$, $q \in \{1, 2, \cdots, N\}$.

As a typical example, considering a service room of dimension $(5 \times 5 \times 3)\,\mathrm{m}$ with the activated LED is located at $(2.5, 2.5, 3.0)\,\mathrm{m}$. Fig. 3 depicts the maximum delay spread Δt of signal paths reflected by different mirrors during a transmission, where the channel impulse response of the indoor VLC system depends on the location of the receiver and varies by moving it on the floor in the considered room. As demonstrated in Fig. 3, the maximum delay spread Δt for the system under consideration varies from $0.2\,\mathrm{ns}$ to $2\,\mathrm{ns}$.

In general, the limitation of ISI is determined by the transmission scenario and the room properties in our considered system and can be quantified by evaluating the channel cut-off frequency [26]. Consider an LED modulation bandwidth of $40\ \mathrm{MHz}$, so the Nyquist symbol period is limited to $12.5\ \mathrm{ns}$, and ISI will occur if transmitted data symbols experience delays larger than $6.25\ \mathrm{ns}$. Simulation results provided in Fig. 3 showed that the maximum delay spread is less than $2\ \mathrm{ns}$, which is significantly below the $6.25\ \mathrm{ns}$. As a result, in the process of system information transmission, the influence of multipath fading and ISI can be almost ignored.

Consequently, for the sake of simplicity, we will neglect all the diffuse propagation NLoS components, this is, consider only the specular reflection path of the mirror array when LoS is blocked. Then, the received signal intensity will depend on the emitter radiation pattern,

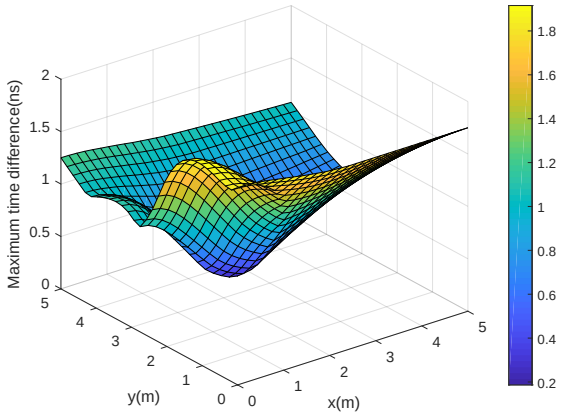

Fig. 3. Maximum delay spread caused by the mirror array in all the service area

characteristics of the receiver, active area of PD, and the reflection coefficient of the mirror. Denoting that the emitted optical intensity is P_T, and the received optical power $P^{(\mathrm{MI})}$ and the channel DC gain $H^{(\mathrm{MI})}(0)$ can be respectively expressed as

$$P^{(\mathrm{MI})} = H^{(\mathrm{MI})}(0)\, P_T, \tag{20}$$

$$H^{(\mathrm{MI})}(0) = \int_{-\infty}^{\infty} h^{(\mathrm{MI})}(t)\, dt. \tag{21}$$

IV. Detection algorithms of mirror array aided indoor SSK-VLC system

A. ML detection algorithm

At present, most signal detection algorithms of indoor VLC system are based on ML, which has the best performance [27]. In SSK-VLC system, ML means that all LED combination sequences are traversed, and the optimal activated one LED is selected from N_t LEDs to convey information signal. This procedure can be achieved as follows

$$\hat{I} = \underset{I\in\{1,2,\cdots,N_t\}}{\arg\min} \|\mathbf{y} - \mathbf{h}_I s\|^2, \tag{22}$$

where $\hat{I}$ represents the estimated value of activated LED index, and $\mathbf{h}_I$ represents the I-th column channel submatrix of channel matrix $\mathbf{H}$, and s is a constant factor used for satisfying the power constraint.

B. OMP detection algorithm based on sparsity

Although the ML detector is optimal, the computational complexity of the exhaustive search increases sharply with the increasing number of transmitting LEDs [28]. In a typical indoor MIMO SSK-VLC system, considering the sparse characteristics of SSK transmitting signals, the sparse signal reconstruction method in CS theory can provide an ideal balance between computational complexity and system performance. This subsection aims to achieve a sparsity aided OMP signal detection algorithm with low complexity and good performance at the receiving end.

In order to uniquely map sparse signals to the output signal space, it is necessary to design an ideal measurement matrix. That is, to recover original signals efficiently, the prerequisite is that the measurement matrix $\mathbf{H}$ must meet RIP properties [29]. However, in our considered indoor MIMO SSK-VLC system, the channel matrix elements are fixed, which leads to disobeying the RIP property of the measurement matrix. Hence, in order to utilize a sparsity aided OMP detection algorithm, an SVD approach is adopted to preprocess the measurement matrix $\mathbf{H}$ [17]. For measurement matrix $\mathbf{H}$, the SVD is given as

$$\mathbf{H} = \mathbf{U}\mathbf{\Sigma}\mathbf{V}^{\mathbf{T}}, \tag{23}$$

where $\mathbf{U}$ and $\mathbf{V}$ are unitary matrices, and $\mathbf{U} \in \mathbb{R}^{N_r \times N_r}$, $\mathbf{V} \in \mathbb{R}^{N_t \times N_t}$, $\mathbf{\Sigma} = [\mathbf{\Delta}, \mathbf{O}]$, $\mathbf{\Delta} = \operatorname{diag}[\gamma_1, \gamma_2, \cdots, \gamma_{N_r}]$, where $\mathbf{O} \in \mathbb{R}^{N_r \times (N_t - N_r)}$ is zero matrix. After preprocessing the measurement matrix $\mathbf{H}$, the received signal can be formulated as

$$\mathbf{y}_{\mathrm{SVD}} = \mathbf{\Delta}^{-1}\mathbf{U}^T\mathbf{y} = \mathbf{Z}\mathbf{x} = \mathbf{H}_{\mathrm{SVD}}\mathbf{\Phi}\mathbf{x} = \mathbf{H}_{\mathrm{SVD}}\mathbf{x}_{\mathrm{SVD}}, \tag{24}$$

where $\mathbf{Z} = \mathbf{\Delta}^{-1}\mathbf{U}^T\mathbf{H} = \left[\mathbf{I}^{N_r \times N_r}, \mathbf{O}\right]\mathbf{V}^T$ is defined as a partial orthogonal matrix, $\mathbf{H}_{\mathrm{SVD}}$ is defined by $\mathbf{Z}$, and the column vectors of $\mathbf{Z}$ are $\mathbf{z}_1, \mathbf{z}_2, \cdots, \mathbf{z}_{N_t}$. Finally, the preprocessed measurement matrix can be expressed as

$$\mathbf{H}_{\mathrm{SVD}} = \mathbf{Z}\mathbf{\Gamma} = \mathbf{Z}\mathbf{\Phi}^{-1}, \tag{25}$$

where $\mathbf{\Gamma} = \operatorname{diag}\left[\left\|\frac{1}{\mathbf{z}_1}\right\|, \left\|\frac{1}{\mathbf{z}_2}\right\|, \cdots, \left\|\frac{1}{\mathbf{z}_{N_t}}\right\|\right]$,$\|\cdot\|$ is the Euclidean norm of a vector and $\mathbf{x}_{\mathrm{SVD}} = \mathbf{\Phi}\mathbf{x}$. Following this, the estimation of the original signal can be attained by correctly reconstructing $\mathbf{x}_{\mathrm{SVD}}$ using OMP sparse reconstruction algorithm as

$$\hat{\mathbf{x}} = \mathbf{\Gamma}\mathbf{x}_{\mathrm{SVD}}. \tag{26}$$

After this preprocessing on the measurement matrix, the classical OMP algorithm can be applied directly as proposed in Table I [17]. In a little more detail, the inner product of

TABLE I

THE OMP DETECTOR PROCEDURE OF INDOOR MIRROR ARRAY AIDED SSK-VLC SYSTEM

Input:	$\mathbf{H}_{\text{SVD}}, \mathbf{y}_{\text{SVD}}$
Output:	$\hat{\mathbf{x}}$, Λ
1.	$\mathbf{r}_0 \leftarrow \mathbf{y}_{\text{SVD}}, t \leftarrow 0, \Lambda_0 \leftarrow \varnothing, \mathbf{A}_0 \leftarrow \varnothing$
2.	while $t \leq n_a$ do
3.	$\mathbf{p} \leftarrow \mathbf{H}_{\text{SVD}}^T \mathbf{r}^{(t-1)}, \mathbb{S}_t \leftarrow \arg\max(\mathbf{p})$
4.	$\Lambda_t = \mathbb{S}_t \cup \Lambda_{t-1}$, $\mathbf{A}_t = \mathbf{H}_{\text{SVD},\Lambda_t} \cup \mathbf{A}_{t-1}$
5.	$\hat{\mathbf{x}}_t = \arg\min \|\mathbf{y}_{\text{SVD}} - \mathbf{A}_t\mathbf{x}\|_2^2 = (\mathbf{A}_t^T \mathbf{A}_t)^{-1} \mathbf{A}_t^T \mathbf{y}_{\text{SVD}}$
6.	$\mathbf{r}_t = \mathbf{y}_{\text{SVD}} - \mathbf{A}_t \hat{\mathbf{x}}_t$
7.	end while

measurement matrix $\mathbf{H}_{\text{SVD}}$ and residual $\mathbf{r}$, denoted as $\mathbf{p}$, is calculated in each iteration. Then the index of the maximum absolute value of $\mathbf{p}$ is selected and put into the set $\mathbb{S}_t$, and then the index set Λ_t and atomic support set matrix $\mathbf{A}_t$ are updated. Additionally, $\mathbf{H}_{\text{SVD},\Lambda_t}$ denotes a submatrix of $\mathbf{H}_{\text{SVD}}$ with columns indices selected from the set Λ_t, and $(\cdot)^T$ denotes the transpose of a matrix or vector. Then, the least squares method is utilized to estimate the signal $\hat{\mathbf{x}}_t$, and the residual is finally updated. The above process is repeated until the end of the iteration of the OMP algorithm.

C. Complexity analysis

Since both the signal and the channel matrix in the considered indoor SSK-VLC system are positive real numbers, we analyzed the complexity of the ML and CS assisted sparse signal reconstruction algorithms from the perspective of floating point operations (flops). The specific complexity calculation is shown in Table II.

TABLE II

COMPUTATION COMPLEXITY ANALYSIS OF ML AND OMP DETECTORS

Detectors	Real-valued flops
ML	$(2N_rN_t + 2N_r - 1)2^{\kappa}$
OMP	$(N_t\,(2N_r - 1) + 7N_r - 1)$

It should be noted that parameter κ in the ML detection algorithm represents the spectrum efficiency in the ML detector of the considered system. Because the complexity of SVD computation is $4N_t^2N_r + 22N_r^3$, which belongs to the same computational level of matrix

inversion, and SVD preprocessing requires only one operation. In our simulations, the number of symbols is set greater than 10^5, and the number of flops of ML is greater than $10^5 \times (2N_rN_t + 2N_r - 1)2^\kappa$, hence the complexity of SVD is negligible.

V. Simulations and Numerical Results

In this section, to demonstrate the performance of the proposed mirror array aided indoor SSK-VLC system, we provide numerical results for an indoor VLC environment having the dimensions of $[5 \times 5 \times 3]$ m^3, represented by a three-dimensional (3D) Cartesian coordinate system $[O_X, O_Y, O_Z]$, and the configuration scheme is considered: $N_t = 9, N_r = 4$. Assuming that the transmit LEDs are perpendicular to the ceiling and down-facing to the floor. Similarly, the PDs of receivers are located on the floor, which is assumed to be perpendicular to the floor and facing the ceiling. Unless otherwise stated, we assume that all simulations are performed in an LoS-blocking environment and include only mirror array-assisted VLC components. Moverover, in most practical cases, the effect of the diffuse component is masked by the mirror-assisted VLC link, as shown in Fig. 5, we also assume that simulation parameters are provided in Table III. Finally, all simulation parameters are converted into a coordinate system with the origin being in one corner of the room. For the first scheme, the LED's position is given in Table IV, and two scenarios of receiver power are considered: the received power of mirror array aided link with that of the LoS link and diffuse reflection link, respectively. The impact of different detector locations in the service space on the received power is investigated.

Fig. 4 demonstrates the PD's received power ratio of the mirror array aided link and that of the LoS link, where the location of the activated LED is $(2.5, 2.5, 3.0)$ m. Furthermore, the position of the mirror array can be determined according to the coordinates of the first mirror in Table III. Observe that the received power ratio is increased in the service area near the wall equipped with a mirror array. We can also observe that the received power gain has a significant improvement when users are near the location of the mirror array, which approaches its maximum about of 5 times the LoS transmission. We can also infer from the results of Fig. 4 that the received power gain of the SSK-VLC system has a relatively high correlation with the user's location. When the user's location is far away from the mirror array, the improvement of receiving power gain is not obvious due to the influence of path fading. However, this can be alleviated by arranging two or more mirror arrays at different walls in the service space. Consequently, the mirror array aided VLC link has a comparable

TABLE III

SIMULATION PARAMETERS

Simulation setup parameters	Values
The area of the mirror, ΔA	$25\ \mathrm{cm}^2$
The area of the PD, A	$1\ \mathrm{cm}^2$
FOV of PD	80°
Width of mirror, w	5 cm
Length of mirror, h	5 cm
Transverse spacing of mirror Δw	5 cm
Longitudinal spacing of mirror Δh	5 cm
Number of mirrors, $M \times N$	6×8
Transmitting power, P_T	20 W
Semi-angle at half power, $\Phi_{1/2}$	75°
Reflection coefficient of the mirror, ρ_{MI}	0.95
Reflection coefficient of diffuse reflection, ρ	0.4
The coordinates of the first mirror	$(0.0, 2.0, 1.5)$ m

TABLE IV

THE DISTRIBUTIONS OF THE LEDS' AND PDS' LOCATIONS

Configuration		PD2	$(2.00, 2.51, 0.80)$ m
9 LEDs	(A_X, A_Y, A_Z)	PD3	$(2.01, 2.50, 0.80)$ m
LED1	$(1.00, 1.00, 3.00)$ m	PD4	$(2.01, 2.51, 0.80)$ m
LED2	$(1.00, 2.00, 3.00)$ m	Scenario 2	
LED3	$(1.00, 3.00, 3.00)$ m	PD1	$(2.50, 2.50, 0.80)$ m
LED4	$(2.00, 1.00, 3.00)$ m	PD2	$(2.50, 2.51, 0.80)$ m
LED5	$(2.00, 2.00, 3.00)$ m	PD3	$(2.51, 2.50, 0.80)$ m
LED6	$(2.00, 3.00, 3.00)$ m	PD4	$(2.51, 2.51, 0.80)$ m
LED7	$(3.00, 1.00, 3.00)$ m	Scenario 3	
LED8	$(3.00, 2.00, 3.00)$ m	PD1	$(3.00, 3.00, 0.80)$ m
LED9	$(3.00, 3.00, 3.00)$ m	PD2	$(3.00, 3.01, 0.80)$ m
4 PDs	(A_X, A_Y, A_Z)	PD3	$(3.01, 3.00, 0.80)$ m
Scenario 1		PD4	$(3.01, 3.01, 0.80)$ m
PD1	$(2.00, 2.50, 0.80)$ m		

performance to the LoS link.

Fig. 5 depicts the received power ratio of the mirror array aided link and that of the NLoS link. Observe from Fig. 5 that the received power ratio of the mirror array assisted link and diffuse reflection link is significant. This owns to the principle of Snell, that is, specular reflection can almost reflect light without loss. However, the diffuse reflection link has a

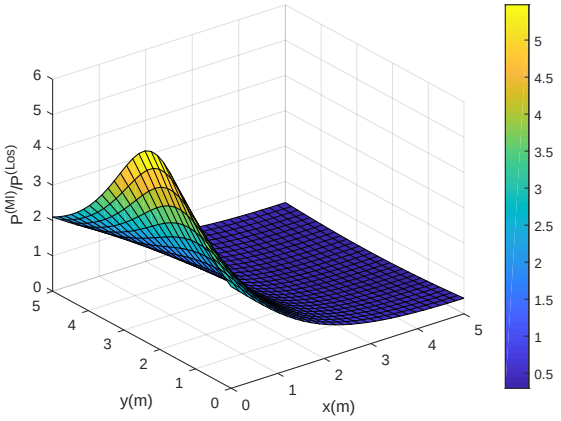

Fig. 4. Received power ratio of the mirror array aided link and that of the LoS link.

large power loss. Moreover, we can also observe from the results of Fig. 5 that the received power gain of the SSK-VLC system has a strong correlation with the mirror array's location. Specifically, when a user is located near the wall equipped with a mirror array, the received power ratio is relatively large compared to other positions in the service space. Because the locations can receive diffuse reflection power from three walls, while the corners and edges can only receive diffuse reflection power from one or two walls, there exists the abrupt change in power ratio of NLoS link at corners, i.e. positions (0,0), (0,5), (5,0) and (5,5), as well as the edges.

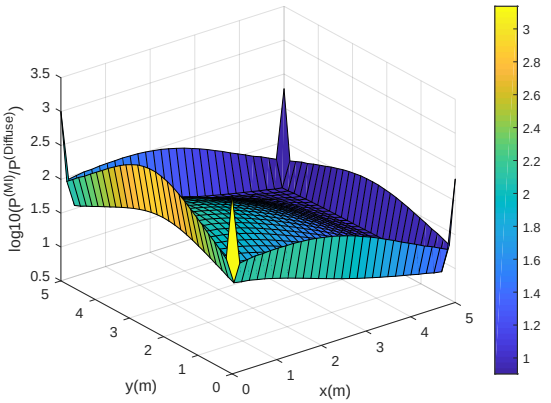

Fig. 5. Received power ratio of the mirror array aided link and that of the NLoS link.

In order to further evaluate the considered scheme, different room shapes and sizes are considered, as well as different locations of the receiver. Since rooms are usually regular

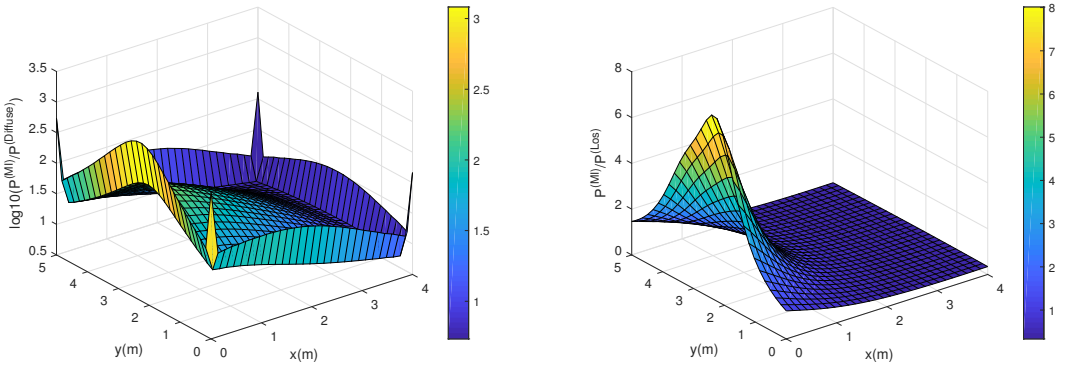

(a) Received power ratio of mirror array assisted link and that of the diffuse reflection link.

(b) Received power ratio of mirror array assisted link and that of the LoS link.

Fig. 6. Rectangle room with size $(4 \times 5 \times 3)$ m.

rectangles or squares in our life, we mainly consider rectangular and square room shapes. Hence we will explore three rooms with different shapes and sizes, which are $(4 \times 5 \times 3)$ m, $(5 \times 5 \times 5)$ m, and $(7 \times 7 \times 3)$ m, respectively. The distribution of 9 LEDs in this simulation is shown in Table IV. The coordinate of the first mirror in the mirror array with respect to the considered coordinate system is $(0.0, 2.0, 1.5)$ m. Other main simulation parameters for the considered SSK VLC system are shown in Table III. Fig. 6, Fig. 7 and Fig. 8 provide the user's received power ratio of the mirror array assisted link and that of the LoS link in all these three scenarios. Furthermore, the received power ratio of the mirror array assisted link and that of the diffuse reflection link is provided in Fig. 6, Fig. 7 and Fig. 8 as well. As can be seen from Fig. 6, Fig. 7 and Fig. 8, not only the received power ratio of the mirror array assisted link and the LoS link is affected by the room size, but also the received power ratio of the mirror array assisted link and the diffuse reflection link is affected by the room size. In a little more detail, in all three scenarios, the received power ratio of the mirror array assisted link and diffuse reflection link is very large. While, when the LoS link is not blocked, the received power ratio of the mirror array assisted link and diffuse reflection link is greatly affected by the distance between the receiver and the mirror array. Specifically, the received power ratio of the mirror array assisted link and that of the LoS link is relatively large when the receiver is near the wall where the mirror array is arranged, while the received power ratio is not significant when the receiver is far away from the wall where the mirror array is arranged.

It is seen that in all cases, the received power can be improved by the proposed mirror

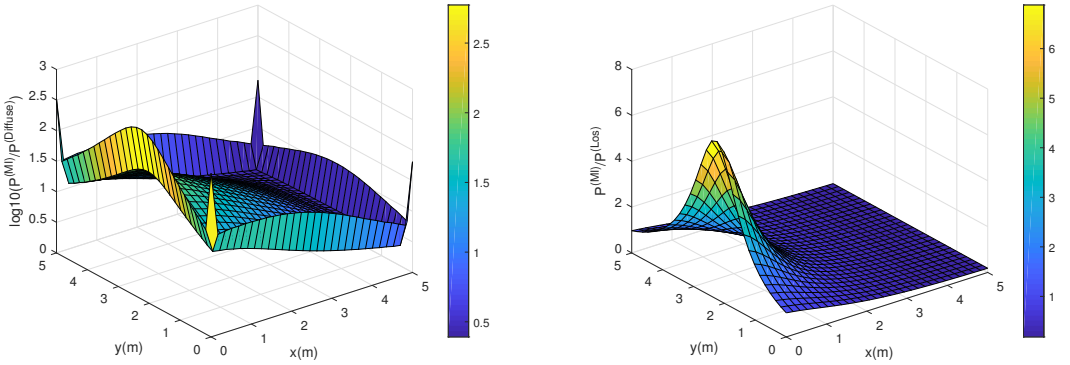

(a) Received power ratio of mirror array assisted link and that of the diffuse reflection link.

(b) Received power ratio of mirror array assisted link and that of the LoS link.

Fig. 7. Square room with size $(5 \times 5 \times 5)$ m.

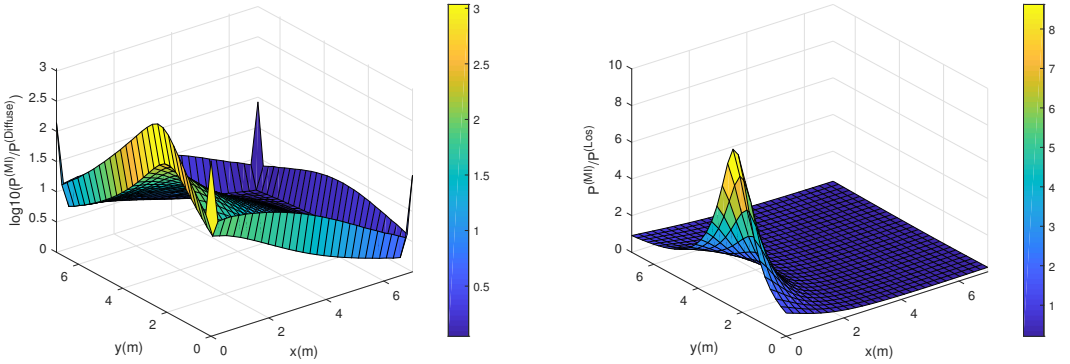

(a) Received power ratio of mirror array assisted link and that of the diffuse reflection link.

(b) Received power ratio of mirror array assisted link and that of the LoS link.

Fig. 8. Square room with size $(7 \times 7 \times 3)$m.

array assisted SSK-VLC system, which is the explicit benefit of the mirror array.

To make the proposed system more convincing, in Fig. 9 we compare the received power with the different number of mirrors in the mirror array by considering the configuration scheme in Table IV. As shown in Fig. 9, upon increasing N, the received power of the detector increases, this attributes to the power focusing characteristic of our proposed mirror array aided SSK-VLC system. As expected, when the number of mirrors increases, more power can be collected. In physical situations, the number N of mirrors can be determined by the requirements of applications.

The BER performance comparisons of the mirror array assisted link and the LoS link are

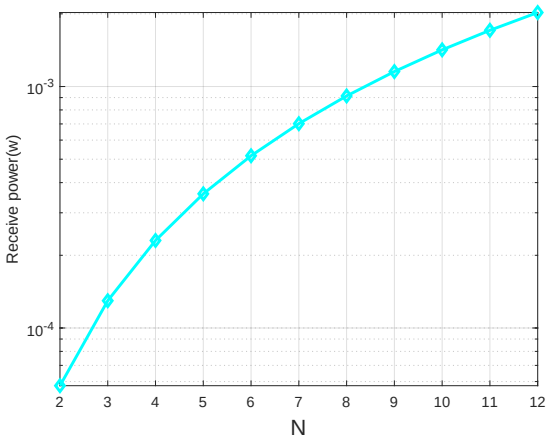

Fig. 9. Received power of the considered mirror array aided indoor SSK-VLC system as the increasing of the number of mirrors $N \times N$.

evaluated in Fig. 10 for two half-power angles of LEDs: $\Phi_{1/2} = 50^\circ$ and 75°. At the same time, three different PDs distributions are considered as well, the detailed parameters are shown in Table IV. Other main simulation parameters of the considered SSK VLC system are shown in Table III and Table IV. Observe from the results shown in Fig. 10 that the BER performance of sparsity aided OMP detector is significantly improved compared to the ML detector. This is because the performance of the ML detector is more likely affected by the correlation between channels. However, for sparsity assisted OMP detector, the performance is mainly affected by the sparsity structure of the channel matrix. For the considered indoor SSK-VLC system, the sparsity structure is apparently determined by activating a single LED to convey information. Moreover, it can also be seen from the results in Fig. 10 that the BER performance of the ML detector and the OMP detector can hardly detect the signal when $\Phi_{1/2} = 50^\circ$. This is because for this limited semi-angle at half power of LED $\Phi_{1/2}$, most of the light emitted by the LED may not be able to illuminate the corresponding mirror array directly. As a result, the BER performance will be improved by increasing $\Phi_{1/2}$. Actually, in practice, in order to guarantee adequate illumination, there are many LEDs equipped on the ceiling of the service environment, furthermore, a relative larger half-power angle of LED $\Phi_{1/2}$ is set. Therefore, we can conclude that the sparsity assisted OMP detector is much more suitable for the considered indoor mirror array aided SSK-VLC system.

Next, to make fair comparisons, the BER performance of ML and OMP are evaluated both with the proposed SVD preprocessing. The main system simulation parameters for the

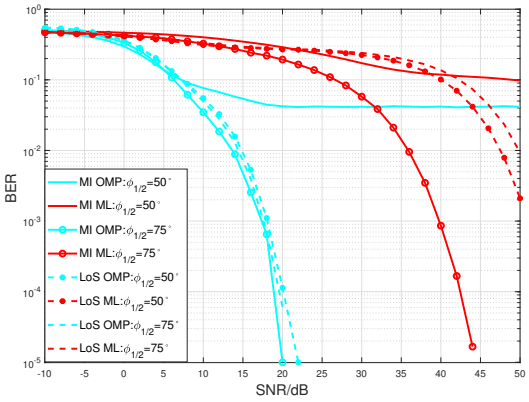

(a) Scenario 1

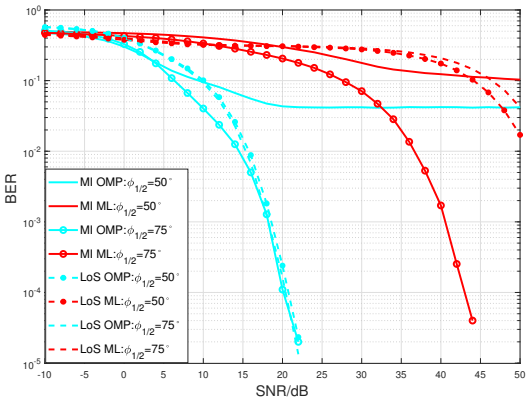

(b) Scenario 2

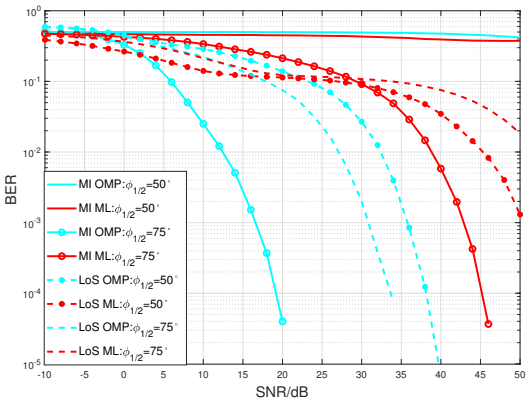

(c) Scenario 3

Fig. 10. The BER performance of ML detector and OMP detector with different half-power angles of LEDs: $\Phi_{1/2} = 50^{\circ}$ and 75°.

considered SSK-VLC system are shown in Table III and Table IV. For mirror array assisted link and LoS link, Fig. 11 depicts the BER performance of the ML detector with and without measurement matrix preprocessing under three scenarios as presented in Table IV, and the BER performance of the proposed OMP detector is presented as well. As can be seen in Fig. 11 that when the ML detection algorithm is also preprocessed by the proposed SVD preprocessing, the BER performance is improved and the SVD aided ML detector has the best BER performance.

Finally, as a function of N_t, Fig. 12 demonstrates the flops ratio of ML detector and OMP detector of the considered SSK-VLC system. As can be seen from Fig. 12, the ML detector has higher complexity compared with SVD assisted OMP detection algorithm under the same parameters setting. Fig. 12 also indicates that the sparsity aided signal detection algorithm is more suitable for large-scale MIMO scenarios with a large number of transmitting LEDs.

VI. Conclusions

In order to alleviate the light blocking problem of LoS downlink in an indoor SSK-VLC system, a mirror array aided scheme is proposed in this paper. In our considered system, the information conveyed by light emitted from the LEDs can be reflected and concentrated to the user's PDs by the mirror array with very few energy losses. Additionally, the multipath fading and ISI issues are analyzed theoretically to address the multipath effects caused by different mirrors. Furthermore, ML and OMP detectors are proposed to achieve signal demodulation and detection, and by the BER performance and computational complexity analysis, the sparsity aided OMP detector has a better performance. Some design parameters are considered in our simulations, such as the half-power angles of LEDs and the number of mirrors. Finally, from the simulation results, it can be seen that the proposed mirror array aided indoor SSK-VLC system can realize downlink even in the LoS link blocking scenarios. We further infer that the sparsity assisted OMP detector is much more suitable for the considered indoor mirror array aided SSK-VLC system.

References

[1] N. Chi, Y. Zhou, Y. Wei, and F. Hu, "Visible light communication in 6G: Advances, challenges, and prospects," *IEEE Vehicular Technology Magazine*, vol. 15, no. 4, pp. 93–102, 2020.

[2] A. Malik and P. Singh, "Free space optics: current applications and future challenges," *International Journal of Optics*, vol. 2015, 2015.

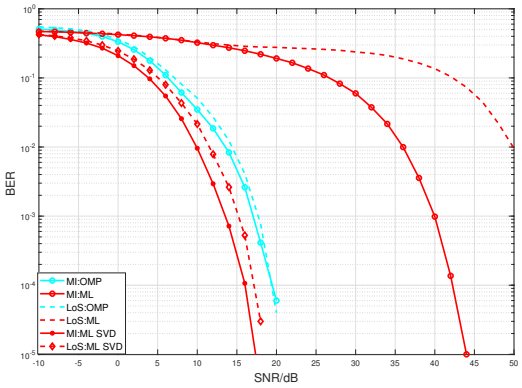

(a) Scenario 1

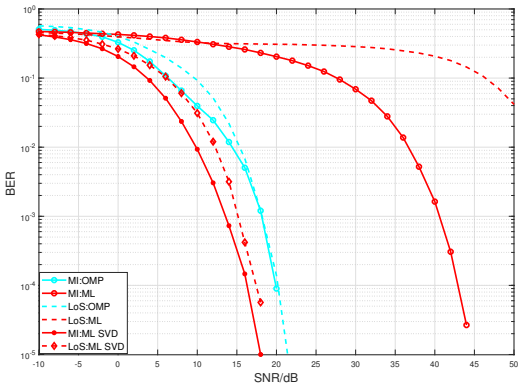

(b) Scenario 2

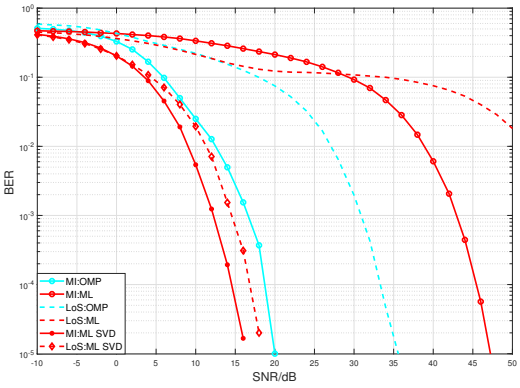

(c) Scenario 3

Fig. 11. BER performance comparisons of the OMP detector and ML detector in three scenarios, where mirror array assisted link and LoS link are considered.

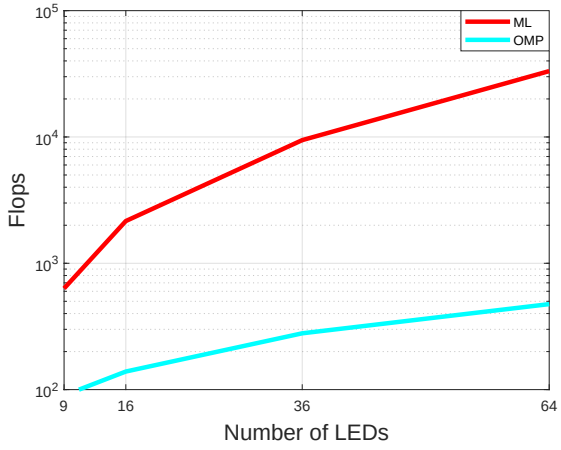

Fig. 12. The number of flops of various detectors as a function of N_t in mirror array aided SSK-VLC system.

[3] F. Zhang, F. Wang, J. Zhang, and T. Zuo, "SVM aided LEDs selection for generalized spatial modulation of indoor VLC systems," *Optics Communications*, vol. 497, p. 127161, 2021.

[4] R. Raj, S. Jaiswal, and A. Dixit, "On the effect of multipath reflections in indoor visible light communication links: Channel characterization and BER analysis," *IEEE Access*, vol. 8, pp. 190 620–190 636, 2020.

[5] H. Wang, F. Wang, and R. Li, "Enhancing power allocation efficiency of NOMA aided-MIMO downlink VLC networks," *Optics Communications*, vol. 454, p. 124497, 2020.

[6] A. Mostafa and L. Lampe, "Physical-layer security for MISO visible light communication channels," *IEEE Journal on Selected Areas in Communications*, vol. 33, no. 9, pp. 1806–1818, 2015.

[7] A. R. Ndjiongue, T. M. N. Ngatched, O. A. Dobre, and H. Haas, "Re-Configurable Intelligent Surface-Based VLC Receivers Using Tunable Liquid-Crystals: The Concept," *Journal of Lightwave Technology*, vol. 39, no. 10, pp. 3193–3200, 2021.

[8] Y. Wu, P. Audenaert, M. Pickavet, and D. Colle, "Mirror-aided non-LOS VLC channel characterizations with a time-efficient simulation model," *Photonic Network Communications*, vol. 38, no. 1, pp. 151–166, 2019.

[9] H. Wang, Z. Zhang, B. Zhu, J. Dang, L. Wu, L. Wang, K. Zhang, Y. Zhang, and G. Y. Li, "Performance Analysis of Multi-Branch Reconfigurable Intelligent Surfaces-Assisted Optical Wireless Communication System in Environment With Obstacles," *IEEE Transactions on Vehicular Technology*, vol. 70, no. 10, pp. 9986–10 001, 2021.

[10] S. Sun, F. Yang, and J. Song, "Sum Rate Maximization for Intelligent Reflecting Surface-Aided Visible Light Communications," *IEEE Communications Letters*, vol. 25, no. 11, pp. 3619–3623, 2021.

[11] S. Aboagye, T. M. N. Ngatched, O. A. Dobre, and A. R. Ndjiongue, "Intelligent Reflecting Surface-Aided Indoor Visible Light Communication Systems," *IEEE Communications Letters*, vol. 25, no. 12, pp. 3913–3917, 2021.

[12] L. Qian, X. Chi, L. Zhao, and A. Chaaban, "Secure Visible Light Communications via Intelligent Reflecting Surfaces," in *ICC 2021 - IEEE International Conference on Communications*, 2021, pp. 1–6.

[13] X. Zhao and J. Sun, "Secure reconfigurable intelligent surface aided heterogeneous VLC–RF cooperative NOMA networks," *Optics Communications*, vol. 511, p. 127983, 2022.

[14] F. Wang, C. Liu, Q. Wang, J. Zhang, R. Zhang, L. Yang, and L. Hanzo, "Optical Jamming Enhances the Secrecy Performance of the Generalized Space-Shift-Keying-Aided Visible-Light Downlink," *IEEE Transactions on Communications*, vol. 66, no. 9, pp. 4087–4102, Sep. 2018.

[15] E. Panayirci, "Optical index-coded space shift keying (IC/SSK)," *IEEE Communications Letters*, vol. 25, no. 8, pp. 2654–2658, 2021.

[16] K. Ying, H. Qian, R. J. Baxley, and S. Yao, "Joint optimization of precoder and equalizer in MIMO VLC systems," *IEEE Journal on Selected Areas in Communications*, vol. 33, no. 9, pp. 1949–1958, 2015.

[17] T. Zuo, F. Wang, and J. Zhang, "Sparsity signal detection for indoor GSSK-VLC system," *IEEE Transactions on Vehicular Technology*, vol. 70, no. 12, pp. 12 975–12 984, 2021.

[18] D. R. Gagnon, "Procedure for correct refocusing of the Rotman lens according to Snell's law," *IEEE transactions on antennas and propagation*, vol. 37, no. 3, pp. 390–392, 1989.

[19] A. M. Abdelhady, A. K. S. Salem, O. Amin, B. Shihada, and M.-S. Alouini, "Visible light communications via intelligent reflecting surfaces: Metasurfaces vs Mirror Arrays," *IEEE Open Journal of the Communications Society*, vol. 2, pp. 1–20, 2021.

[20] P. Dutre, K. Bala, and P. Bekaert, *Advanced global illumination*. AK Peters/CRC Press, 2018.

[21] S. Marschner and P. Shirley, *Fundamentals of computer graphics*. CRC Press, 2018.

[22] J. Carruthers and J. Kahn, "Modeling of nondirected wireless infrared channels," *IEEE Transactions on Communications*, vol. 45, no. 10, pp. 1260–1268, 1997.

[23] T. Komine and M. Nakagawa, "Fundamental analysis for visible-light communication system using LED lights," *IEEE Transactions on Consumer Electronics*, vol. 50, no. 1, pp. 100–107, 2004.

[24] D.-S. Shiu and J. Kahn, "Differential pulse-position modulation for power-efficient optical communication," *IEEE Transactions on Communications*, vol. 47, no. 8, pp. 1201–1210, 1999.

[25] A. M. Abdelhady, O. Amin, A. K. S. Salem, M.-S. Alouini, and B. Shihada, "Channel Characterization of IRS-Based Visible Light Communication Systems," *IEEE Transactions on Communications*, vol. 70, no. 3, pp. 1913–1926, 2022.

[26] J. Grubor, S. Randel, K.-D. Langer, and J. W. Walewski, "Broadband information broadcasting using LED-based interior lighting," *Journal of Lightwave Technology*, vol. 26, no. 24, pp. 3883–3892, 2008.

[27] J. Jeganathan, A. Ghrayeb, and L. Szczecinski, "Spatial modulation: Optimal detection and performance analysis," *IEEE Communications Letters*, vol. 12, no. 8, pp. 545–547, 2008.

[28] W. O. Popoola and H. Haas, "Demonstration of the merit and limitation of generalised space shift keying for indoor visible light communications," *Journal of Lightwave Technology*, vol. 32, no. 10, pp. 1960–1965, 2014.

[29] J. A. Tropp and A. C. Gilbert, "Signal recovery from random measurements via orthogonal matching pursuit," *IEEE Transactions on information theory*, vol. 53, no. 12, pp. 4655–4666, 2007.